JBC RESEARCH ARTICLE

Disentangling autoproteolytic cleavage from tethered agonist–dependent activation of the adhesion receptor ADGRL3

Received for publication, August 22, 2022, and in revised form, October 7, 2022 Published, Papers in Press, October 14, 2022,
https://doi.org/10.1016/j.jbc.2022.102594

Nicole A. Perry-Hauser[1,2], **Max W. VanDyck**[3], **Kuo Hao Lee**[4], **Lei Shi**[4], **and Jonathan A. Javitch**[1,2,*]

From the [1]*Departments of Psychiatry and Molecular Pharmacology and Therapeutics, Columbia University Vagelos College of Physicians and Surgeons, New York, New York, USA;* [2]*Division of Molecular Therapeutics, New York State Psychiatric Institute, New York, New York, USA;* [3]*Department of Biochemistry, Vassar College, Poughkeepsie, New York, USA;* [4]*Computational Chemistry and Molecular Biophysics Section, Molecular Targets and Medications Discovery Branch, National Institute on Drug Abuse-Intramural Research Program, National Institutes of Health, Baltimore, Maryland, USA*

Edited by Kirill Martemyanov

Adhesion G protein-coupled receptor latrophilin 3 (ADGRL3), a cell adhesion molecule highly expressed in the central nervous system, acts in synapse formation through *trans* interactions with its ligands. It is largely unknown if these interactions serve a purely adhesive function or can modulate G protein signaling. To assess how different structural elements of ADGRL3 (*e.g.*, the adhesive domains, autoproteolytic cleavage site, or tethered agonist (TA)) impact receptor function, we require constructs that disrupt specific receptor features without impacting others. While we showed previously that mutating conserved Phe and Met residues in the TA of ADGRL3–C-terminal fragment (CTF), a CTF truncated to the G protein-coupled receptor proteolysis site, abolishes receptor-mediated G protein activation, we now find that autoproteolytic cleavage is disrupted in the full-length version of this construct. To identify a construct that disrupts TA-dependent activity without impacting proteolysis, we explored other mutations in the TA. We found that mutating the sixth and seventh residues of the TA, Leu and Met, to Ala impaired activity in a serum response element activity assay for both full-length and CTF constructs. We confirmed this activity loss results from impaired G protein coupling using an assay that acutely exposes the TA through controlled proteolysis. The ADGRL3 mutant expresses normally at the cell surface, and immunoblotting shows that it undergoes normal autoproteolysis. Thus, we found a construct that disrupts tethered agonism while retaining autoproteolytic cleavage, providing a tool to disentangle these functions *in vivo*. Our approach and specific findings are likely to be broadly applicable to other adhesion receptors.

The adhesion G protein-coupled receptor latrophilins (ADGRL1-3) are highly expressed in the central nervous system. They are best known for their role in synaptic adhesion through *trans* interaction with endogenous interacting partners, notably the teneurins (1) and fibronectin leucine-rich repeat transmembrane proteins (2), which interact with the adhesive N-terminal rhamnose-binding lectin and olfactomedin-like domains, respectively (Fig. 1*A*). In addition to these two adhesion modules, ADGRLs are composed of a serine-/threonine-rich region and hormone receptor motif, a conserved G protein-coupled receptor (GPCR) autoproteolysis-inducing (GAIN) domain that encompasses the GPCR proteolysis site (GPS), and a seven transmembrane (7TM) domain (3–5). Autoproteolytic cleavage at the GPS divides the receptor into an N-terminal fragment (NTF) and a C-terminal fragment (CTF) that remain associated throughout receptor trafficking to the cell surface. The seven residues immediately C-terminal to the GPS (denoted P1′-P7′) (4) constitute the tethered agonist peptide (TA) (also known as the Stachel or stalk peptide), which when exposed binds to the transmembrane domain of ADGRLs and promotes the activation of heterotrimeric G proteins (6–8).

To assess how different structural elements impact the functionality of ADGRL3, we sought to design a mutation that impairs TA-mediated receptor activation but preserves normal autoproteolytic cleavage. Other groups have designed mutants with impaired autoproteolytic cleavage alone, notably with mutations of the proteolysis consensus site, HL/T, such as $T^{P1'}G$ in ADGRLs (5, 9). We previously showed that mutating the conserved $F^{P3'}$ and $M^{P7'}$ TA residues to Ala in ADGRL3 resulted in dramatically impaired G protein activity (7). However, here, we show that this double mutation in the full-length (FL) receptor also disrupts autoproteolysis, making it impossible to use this construct to differentiate the role of disrupted tethered agonism from that of the loss of autoproteolytic cleavage.

Recent work revealed the high-resolution structure of TA-bound ADGRL3-CTF in complex with $miniG_{13}$ heterotrimer (8). Using the structure as a guide, the authors tested a series of critical interactions between the TA and 7TM domain. Notably, the authors observed a dramatic impairment of G protein activation when they mutated $L^{P6'}$ to Ala; so we evaluated this mutant for signaling and cleavage. In addition, we also tested the double mutation of $L^{P6'}$ and $M^{P7'}$ to Ala. We

* For correspondence: Jonathan A. Javitch, jaj2@cumc.columbia.edu.

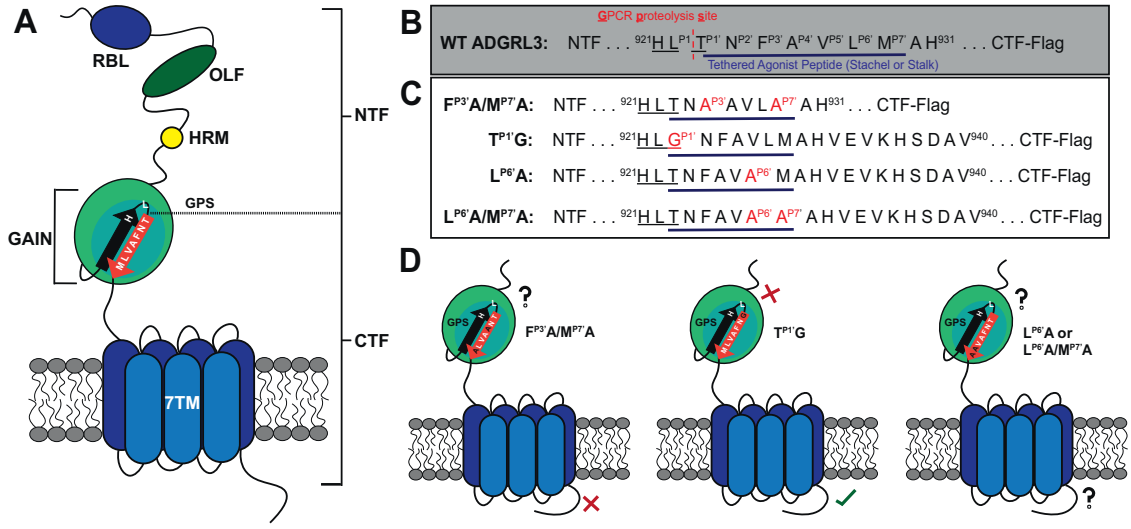

Figure 1. The GPCR proteolytic site undergoes autoproteolytic cleavage to release the tethered agonist and facilitate receptor activation. *A*, cartoon representation of full-length (FL) ADGRL3. The N-terminal fragment (NTF) of the receptor is comprised of rhamnose-binding lectin (RBL) and olfactomedin (OLF) domains, a serine/threonine-rich region, and a hormone receptor motif (HRM). Proteolysis occurs within the GPCR autoproteolysis-inducing domain (GAIN) at the GPCR proteolytic site (GPS). Cleavage occurs between HL^{P1} and $T^{P1'}$, resulting in exposure of the TA peptide. The C-terminal fragment (CTF) of the receptor is composed of a transmembrane GPCR fold (7 TM) that signals through heterotrimeric G proteins. *B–C*, construct design for the ADGRL3 mutants tested in this study. *D*, anticipated functional outcomes for the ADGRL3 mutants tested in this study. The upper denotation represents the receptor's ability to undergo autoproteolytic cleavage, whereas the lower denotation represents TA-mediated receptor activation. ADGRL3, adhesion G protein-coupled receptor latrophilin 3; GPCR, G protein-coupled receptor; TA, tethered agonist; 7 TM, seven transmembrane.

show that ADGRL3-$L^{P6'}A/M^{L7'}A$ undergoes efficient autoproteolytic cleavage but has dramatically impaired TA-mediated receptor activation, whereas the single mutant ADGRL3-$L^{P6'}A$ maintains substantial serum response element (SRE) activity. This double mutation therefore successfully isolates tethered agonism from receptor cleavage, providing an important molecular tool for studying latrophilins and likely other adhesion receptors.

Results

The ADGRL3-$L^{P6'}A/M^{P7'}A$ mutations in the TA impair activity

To find an ADGRL3 construct with impaired TA-dependent activation but preserved autoproteolytic cleavage, we designed three constructs (Fig. 1, *B* and *C*): 1) ADGRL3-$F^{P3'}A/M^{P7'}A$ (7), 2) ADGRL3-$L^{P6'}A$ (8), and 3) ADGRL3-$L^{P6'}A/M^{P7'}A$ (8). We chose ADGRL3-$F^{P3'}A/M^{P7'}A$ as a positive control for impaired TA activity (7) and ADGRL3-$T^{P1'}G$ as a positive control for impaired autoproteolytic cleavage (Fig. 1*D*) (5, 9). We first tested our receptor constructs for impaired receptor activation using a dual-glo SRE luciferase reporter (Fig. 2*A*). We validated the assay by cotransfecting cells with the SRE-luciferase plasmid and increasing concentrations of either FL ADGRL3 or the constitutively active CTF construct (ADGRL3-CTF) (Fig. 2, *B* and *C*). FL ADGRL3 showed increased SRE activity with increasing concentrations of transfected DNA (ranging from ∼5–10 fold). While it is conceivable that this increase in signal may be due to a small fraction of receptors from which the NTF has dissociated, it is also possible that NTF dissociation is not absolutely required for receptor activation. The signal was also greatly enhanced by ADGRL3-CTF (∼25–30 fold), largely independent of DNA concentration in the range tested, consistent with our published work (7).

Mutation of $T^{P1'}G$ in the proteolysis consensus site of the GAIN domain of ADGRL1 was shown to abrogate cleavage (5). The same mutation in human ADGRL3 also abolished autoproteolysis but preserved activity in an SRE-luciferase assay (9). We found that FL ADGRL3-$T^{P1'}G$ showed measurable but diminished receptor activation, whereas ADGRL3-$T^{P1'}G$-CTF demonstrated robust SRE activity, on par or even greater than WT ADGRL3-CTF (Fig. 2, *B* and *C*). Thus, ADGRL3-$T^{P1'}G$ retains a functional TA.

Using the SRE-luciferase assay, we showed that ADGRL3-$F^{P3'}A/M^{P7'}A$ and ADGRL3-$F^{P3'}A/M^{P7'}A$-CTF had disrupted SRE activity compared to WT receptor, suggesting that this receptor construct cannot activate $G\alpha_{12/13}$ (Fig. 2, *B* and *C*). In contrast, while a single mutation of $L^{P6'}$ to Ala led to somewhat diminished signaling in the FL construct, it led to robust SRE activation in the CTF (Fig. 2, *B* and *C*). This is unlike the result previously published for $L^{P6'}A$ using GTPγS turnover with reconstituted $G\alpha_{13}$ (8). However, unlike the turnover assay, which is an acute readout of G protein coupling, the SRE activity assay is downstream of G protein activation and accumulates luciferase over a period of 24 h. Thus, our findings highlight the importance of using multiple assays to assess different aspects of signaling (*i.e.*, acute *versus* extended response). As hypothesized, double mutation of $L^{P6'}A$ and $M^{P7'}A$ fully disrupted SRE activity in both the FL and CTF formats (Fig. 2, *B* and *C*), suggesting the receptors are unable to activate $G\alpha_{12/13}$.

ADGRL3-$L^{P6'}A/M^{P7'}A$ does not couple to $G\alpha_{13}$ in an acute activation assay

To confirm these results with the double mutant at the level of G protein activation, we used a Gβγ release bioluminescence resonance energy transfer (BRET) assay (10) with acute

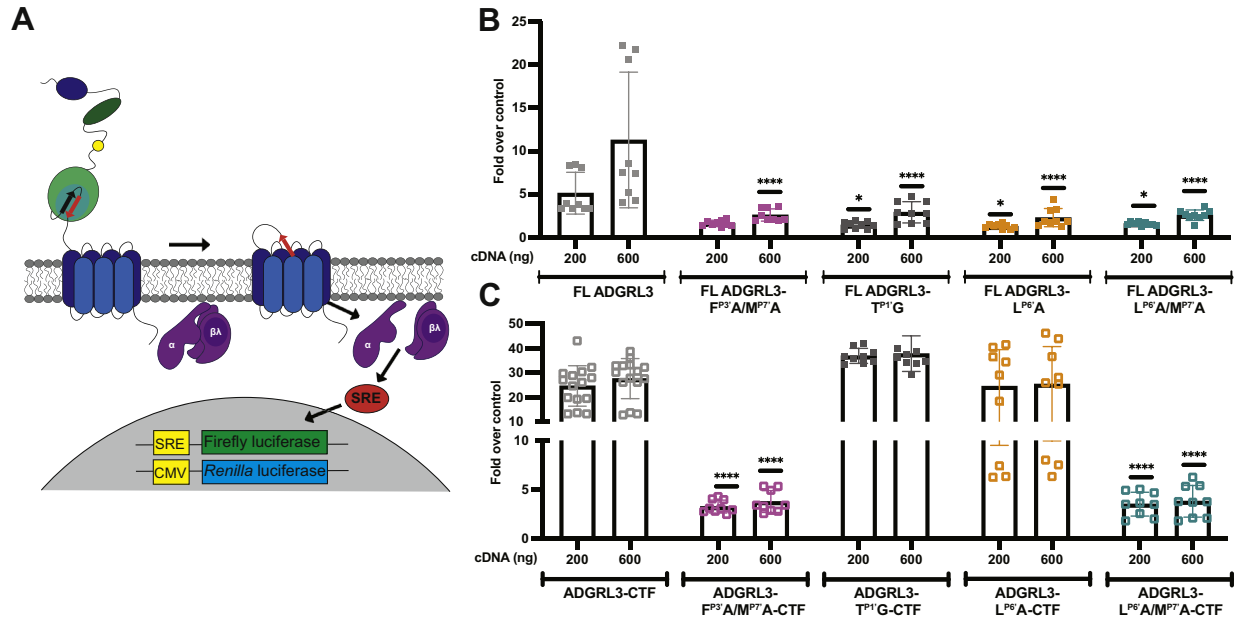

Figure 2. SRE-luciferase activity is disrupted in ADGRL3-L$^{P6'}$A/M$^{P7'}$A. *A*, schematic of the dual-glo serum response element (SRE)-luciferase reporter assay. To activate ADGRL3, the tethered agonist (TA) binds to the orthosteric pocket of the receptor, resulting in the release of Gα and Gβγ subunits from the heterotrimer. This release initiates a cascade of downstream second messenger pathways and eventual gene transcription of firefly luciferase by SRE. As an internal control, *Renilla* luciferase is expressed downstream of the constitutive promoter CMV. *B*, SRE-luciferase assay for full-length ADGRL3 and mutant constructs ADGRL3-F$^{P3'}$A/M$^{P7'}$A, ADGRL3-T$^{P1'}$G, ADGRL3-L$^{P6'}$A, and ADGRL3-L$^{P6'}$A/M$^{P7'}$A. *C*, SRE-luciferase assay for ADGRL3-CTF and mutant constructs ADGRL3-F$^{P3'}$A/M$^{P7'}$A-CTF, ADGRL3-T$^{P1'}$G-CTF, ADGRL3-L$^{P6'}$A-CTF, and ADGRL3-L$^{P6'}$A/M$^{P7'}$A-CTF. Data in (*B*) and (*C*) are expressed relative to the absence of receptor (*control*). Statistics were calculated using the two-way ANOVA with Tukey's multiple comparison test. The mean of the WT receptor control at 200 ng or 600 ng was compared to the mean of the corresponding mutant receptors (*$p < 0.1$; ****$p < 0.0001$). ADGRL3, adhesion G protein-coupled receptor latrophilin 3; CTF, C-terminal fragment.

TA exposure using a protease-activatable ADGRL3 construct (Fig. 3*A*). In contrast to our previous work using thrombin for cleavage (7), which leaves a single residue "scar" at the start of the TA, we adapted a recently published method that uses enterokinase and leaves a native TA (11). Enterokinase recognizes the trypsinogen substrate sequence DDDDK and cleaves after the lysine residue. Thus, we cloned an ADGRL3 construct with the endogenous ADGRL3 signal peptide, a self-labeling protein (SNAP-tag), a flexible linker (GGSGGSGGS), the enterokinase recognition site (DDDDK), and the truncated ADGRL3-CTF sequence. We expressed this receptor construct in a HEK293 cell line with targeted deletion of all G proteins (12) and monitored energy transfer after the addition of enterokinase in the presence and absence of $G\alpha_{13}$. As with our thrombin-activatable construct (7), the enterokinase-cleavable WT ADGRL3 construct gave a robust BRET response after the addition of enterokinase in the presence of $G\alpha_{13}$ compared to its absence (Fig. 3*B*). However, for the cleavable ADGRL3-L$^{P6'}$A and ADGRL3-L$^{P6'}$A/M$^{P7'}$A constructs, enterokinase treatment failed to produce a BRET response even in the presence of $G\alpha_{13}$ (Fig. 3*B*). This suggests that ADGRL3-L$^{P6'}$A and ADGRL3-L$^{P6'}$A/M$^{P7'}$A have greatly impaired acute TA-mediated activation of $G\alpha_{13}$.

ADGRL3-L$^{P6'}$A/M$^{P7'}$A is expressed at the cell surface

To ensure that the ADGRL3-L$^{P6'}$A/M$^{P7'}$A construct was normally expressed, we performed a cell surface–labeling experiment with an impermeant dye targeted to the extracellular SNAP-tag (13, 14) (Fig. 3*C*). We did not detect a significant difference in expression between FL WT ADGRL3 and FL ADGRL3-L$^{P6'}$A/M$^{P7'}$A (Fig. 3*D*). ADGRL3-L$^{P6'}$A/M$^{P7'}$A-CTF was expressed at a somewhat greater level than ADGRL3-CTF (Fig. 3*E*), but even with this higher expression, it was unable to activate $G\alpha_{13}$ (Fig. 3*B*).3

ADGRL3-L$^{P6'}$A/M$^{P7'}$A retains normal autoproteolytic cleavage

We next used an immunoblot assay to test whether the FL versions of our ADGRL3 mutants undergo autoproteolytic cleavage (Fig. 4). We used a primary antibody against the FLAG tag positioned on the C-terminus of the receptor. We expected our FL ADGRL3 constructs to run at ∼173 kDa and the cleaved receptor at ∼71 kDa (Fig. 4*A*). Both our FL ADGRL3-Flag and truncated ADGRL3-CTF-FLAG ran as expected (Fig. 4*B*). The ADGRL3-T$^{P1'}$G-Flag showed banding at only the uncleaved molecular weight, confirming that it does not undergo autoproteolytic cleavage. The ADGRL3-F$^{P3'}$A/M$^{P7'}$A-FLAG construct also showed banding only at the uncleaved position. This was not completely unexpected, as previous work in ADGRL1 showed that a single mutation of F$^{P3'}$ impairs autoproteolytic cleavage (5). Finally, the ADGRL3-L$^{P6'}$A/M$^{P7'}$A-Flag construct showed banding only at the position of cleaved receptors, consistent with robust autoproteolytic cleavage.

Structural basis for disrupted TA-mediated activation and cleavage

To build a structural context for understanding the impaired TA activation of ADGRL3-L$^{P6'}$A/M$^{P7'}$A, we carried

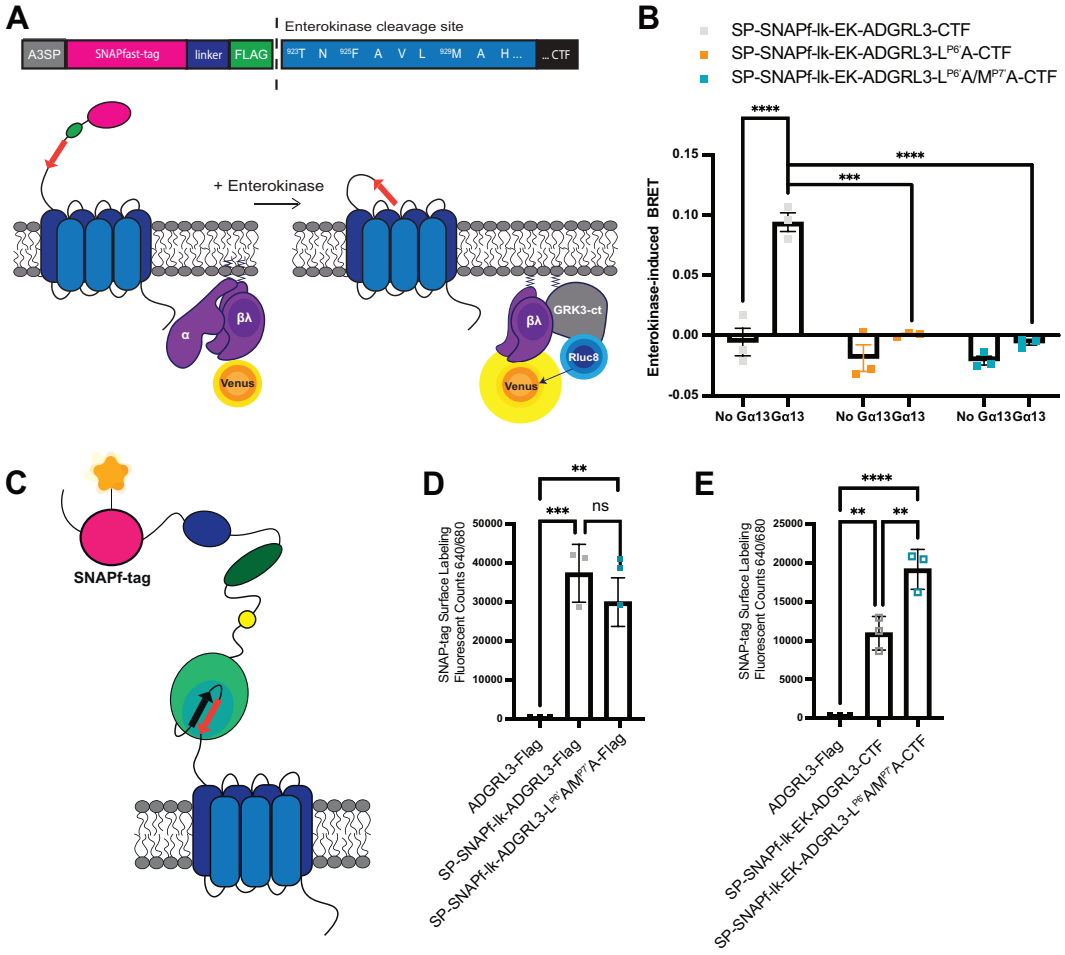

Figure 3. ADGRL3-L$^{P6'}$A/M$^{P7'}$A cannot activate Gα_{13}. *A*, schematic of the Gβγ release bioluminescence energy resonance transfer (BRET) assay. HEK293 cells with targeted deletion of all G proteins (12) were transfected with ADGRL3 cDNA, Gα13, Gβ1, Gγ2-Venus, membrane-anchored GRK3ct-Rluc8, and empty vector pCDNA5/FRT to balance. The protease activatable ADGRL3 constructs contain an ADGRL3 signal peptide, followed by a SNAP-tag, flexible linker, Flag tag, and the ADGRL3-CTF. Upon addition of 5.5 units of enterokinase, the construct is cleaved to acutely expose the tethered agonist and activate G protein. *B*, Gβγ release testing ADGRL3-CTF, ADGRL3-L$^{P6'}$A-CTF, and ADGRL3-L$^{P6'}$A/M$^{P7'}$A-CTF activation of Gα_{13}. Statistics were calculated using ordinary one-way ANOVA with Sidak's multiple comparison test to compare each cell mean with the other cell mean in that column. This analysis was then followed by multiple unpaired t tests to compare the WT receptor to the two mutant constructs (***$p < 0.001$; ****$p < 0.0001$). *C*, cartoon representation of the full-length (FL) ADGRL3 receptor labeled with impermeant Janelia Fluor 646. *D*, fluorescent counts for FL ADGRL3, SNAP-ADGRL3, and SNAP-ADGRL3-L$^{P6'}$A/M$^{P7'}$A. *E*, fluorescent counts for FL ADGRL3, SNAP-ADGRL3-CTF, and SNAP- ADGRL3-L$^{P6'}$A/M$^{P7'}$A-CTF. The same negative control values were used for FL and CTF expression comparisons. Statistics for SNAP-tag labeling were calculated using ordinary one-way ANOVA with Tukey's multiple comparison test (ns, not significant; **$p < 0.01$; ***$p < 0.001$; ****$p < 0.0001$). ADGRL3, adhesion G protein-coupled receptor latrophilin 3; CTF, C-terminal fragment.

out molecular dynamic (MD) simulations based on the cryo-EM structure of the ADGRL3/$G_{\alpha13}$ complex (8), both for the WT and the double mutant receptor. In comparison to WT, the L$^{P6'}$A/M$^{P7'}$A mutation altered the orientation of W1158 at the bottom of the binding pocket (Fig. 5, *A*–*C*). This conformational rearrangement is likely due to the space created by the mutations, which allows the χ1 rotamer of W1158 to rotate from *gauche*+ to *trans*, whereas the interaction with M$^{P7'}$ retains the *gauche*+ rotamer of W1158 in WT (Fig. 5*E*). Consequently, and in combination with other disruptive effects of the mutations, the TA was shifted upwards in the binding pocket, as demonstrated by the increased distance between residues L$^{P6'}$ and F1092 and the decreased distance between residues M$^{P7'}$ and F995 (Fig. 5*D*). To validate the importance of the interaction of the TA with W1158, we generated a W1158A mutant and assessed signaling in the SRE activity and BRET assays (Fig. 5, *F* and *G*). Both assays showed greatly impaired signaling, suggesting that W1158 plays a role as a toggle switch, similar to the role of Trp$^{6.48}$ in class A GPCRs (15).

Structural analysis of the ADGRL1 GAIN domain (Fig. 5*H*) suggests that F$^{P3'}$ likely stabilizes the turn between the two β-strands in the GAIN domain where autoproteolysis occurs between L^{P1} and T$^{P1'}$ and forms an aromatic-hydrophobic interaction with T$^{P1'}$ (Fig. 5*I*). Disruption of these interactions by mutation of F$^{P3'}$, therefore, disrupts cleavage, whereas mutation of the L$^{P6'}$ likely preserves essential hydrophobic interactions and allows cleavage.

Discussion

Adhesion GPCRs are challenging to study, largely due to their structural complexity and the lack of robust pharmacological tools to activate or inhibit their actions. Specific to

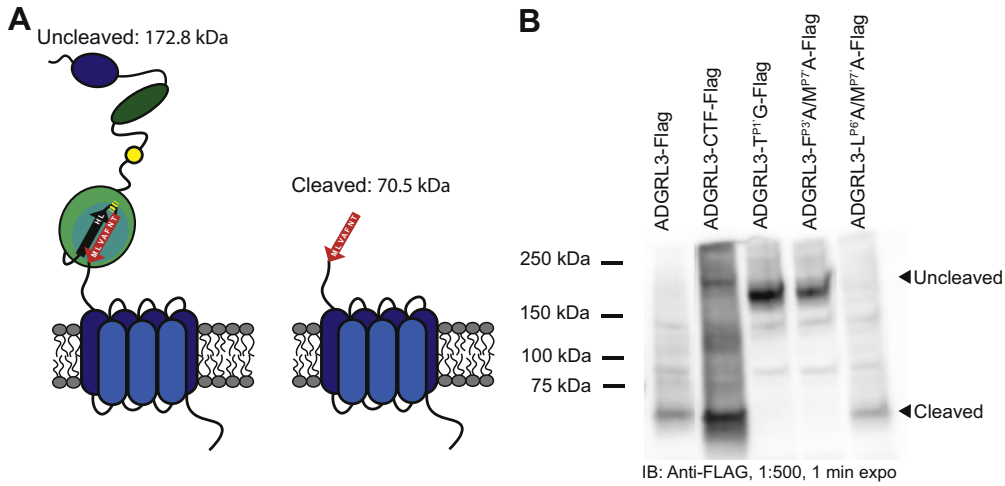

Figure 4. ADGRL3-L$^{P6'}$A/M$^{P7'}$A retains normal autoproteolytic cleavage. *A*, expected molecular weights for the uncleaved and cleaved receptors are 172.8 kDa and 70.5 kDa, respectively. *B*, representative immunoblot against primary Flag (1:500, Thermo Fisher Scientific, PA1-984B) and secondary anti-rabbit IgG-HRP (1:10,000, Thermo Fisher Scientific, Cat #31458). ADGRL3, adhesion G protein-coupled receptor latrophilin 3.

ADGRL3, gene disruption across animal species causes hyperactivity and alters dopaminergic neurotransmission (16–22). Thus, ADGRL3 may offer a novel target for modulating dopaminergic neurotransmission, but the molecular mechanisms underlying this regulation remain unknown. To elucidate these mechanisms *in vivo* requires receptor constructs that selectively disrupt the various structural and functional elements of the receptor. While several studies have reported ADGRL3 constructs that disrupt either cell–cell adhesion (23–25) or autoproteolytic cleavage (9), we were unable to find a published construct that impaired TA-mediated receptor activation without impacting autoproteolysis. Here, we describe a double mutation in ADGRL3, ADGRL3-L$^{P6'}$A/M$^{P7'}$A, that retains normal cleavage but has impaired TA activity and G protein coupling and provides a structural context for our findings. This engineered receptor will be useful in determining how autoproteolytic cleavage and TA activity individually impact ADGRL3 function *in vivo* in the context of the FL receptor, and its design can likely be applied to other adhesion G protein-coupled receptors (aGPCRs).

The relative contributions and/or necessity of autoproteolytic cleavage and the tethered agonist to aGPCR activity remain an area of active study and substantial contention. Several published studies have attempted to unravel the mechanistic details of aGPCR action *in vivo* (26–29). However, current reports that use mutagenesis to impair tethered agonist activity have largely ignored the effect of mutations on autoproteolytic cleavage. Essentially, all published mutations used to disrupt TA activity involve the P3′ position and thus are likely to prevent cleavage in the FL constructs. While these mutations are useful in the context of studying the function of the isolated CTF, they create an unappreciated confound in the context of the FL receptor. Isolating tethered agonism from autoproteolytic cleavage, which we have accomplished here for the first time, will simplify analysis of *in vivo* results and provide powerful support for how these receptor features impact biological systems.

There are several adhesion GPCRs that cannot undergo autoproteolysis: ADGRE1, ADGRA2/A3, ADGRC1/C3, ADGRD2, ADGRF2, ADGRF4, and ADGRG7 (4). Impaired autoproteolysis is typically the result of an altered GPS. For example, minimal to no autoproteolysis occurs for receptors that lack a basic residue at P2 (*e.g.*, Arg/Lys/His) or a polar residue at P1′ (*e.g.*, Ser/Tyr/Asn/Gln/Cys/Thr). Some of these noncleaved aGPCRs are still capable of signaling; therefore, activation does not seem to be completely dependent on tethered agonist exposure through removal of the NTF (6, 30). MD simulations of spontaneous TA exposure have recently been reported for five intact aGPCR homologs (ADGRB3, ADGRE2, ADGRE5, ADGRG1, and Lphn1) (31). This study used biorthogonal labeling of conserved positions within the TA to show that large portions (+6 residues) of the TA can become solvent accessible in the context of the GAIN domain. Thus, it is possible that an intact aGPCR heterodimer could unmask the TA sufficiently for interaction with the 7 TM, resulting in receptor activation, and this might also occur for an uncleaved construct to an extent sufficient for signaling. A recent report indicates that an uncleaved knock-in construct of ADGRF5 fails to rescue function *in vivo* (27). This contrasts with our work using ADGRL2, in which we show that an uncleaved receptor with an intact TA retains intermediate function relative to WT, whereas an uncleaved TA with a dead TA is without function (29). Thus, the field is complex and requires constructs like those we have developed here to evaluate these questions systematically *in vitro* and *in vivo*.

Experimental procedures

Plasmid DNA constructs

FL mouse ADGRL3 cDNA was used as a template in PCR to make the described ADGRL3 constructs on a pcDNA3.1+ backbone. Plasmids were assembled by Gibson assembly using NEBuilder HiFi DNA Assembly Master Mix (New England

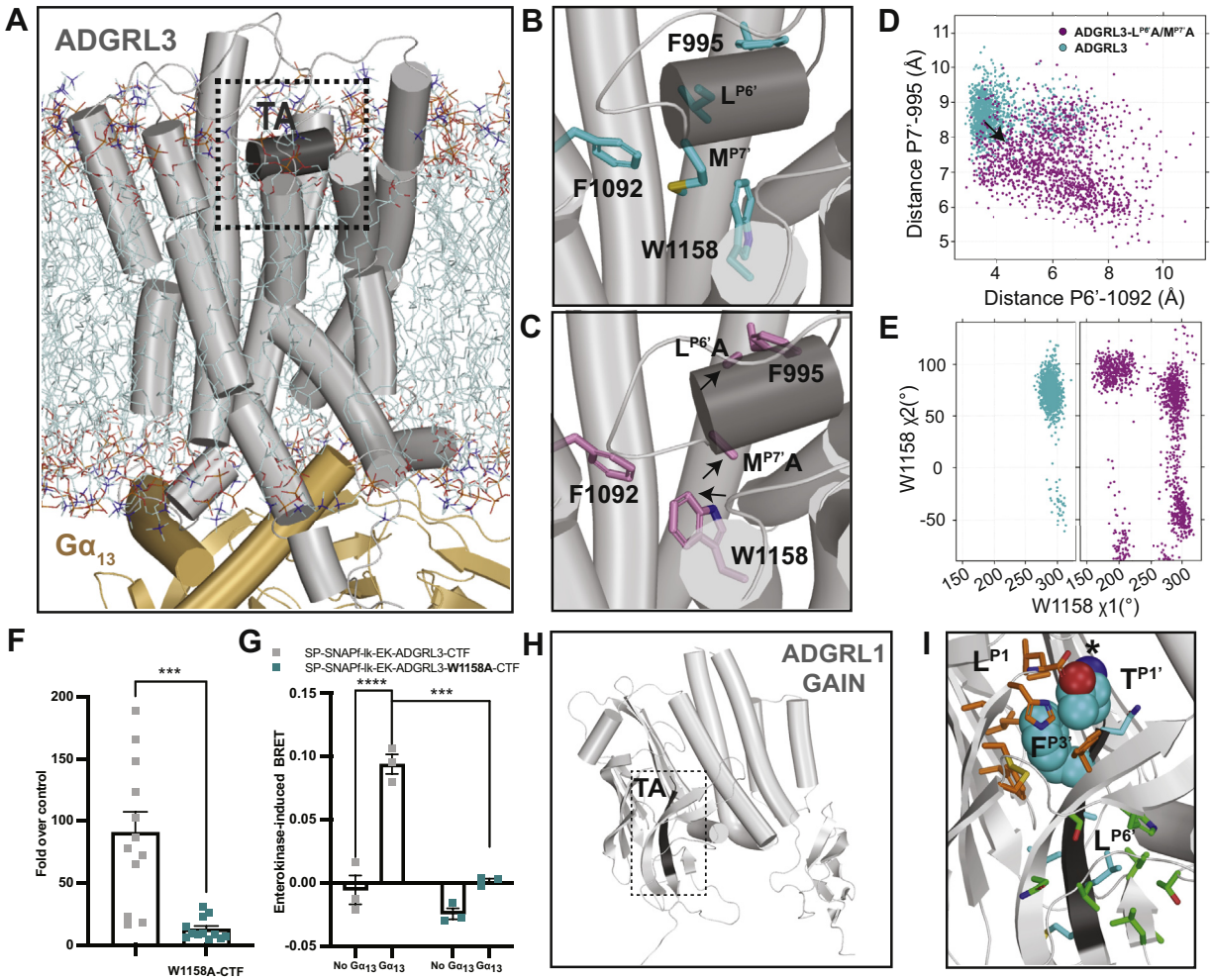

Figure 5. The $L^{P6'}A/M^{P7'}A$ mutation weakens the interactions of the TA in the binding pocket. *A*, the molecular dynamics (MD) simulation system of the human ADGRL3/G protein complex embedded in a lipid bilayer. The receptor, G protein, and lipid bilayer are colored in *gray*, *gold*, and *cyan*, respectively. The tethered agonist (TA) is highlighted with *dark gray*. *B–C*, the resulting conformations of the TA and several key residues in the binding pocket of ADGRL3 (*cyan*) and ADGRL3-$L^{P6'}A/M^{P7'}A$ (*magenta*), respectively. The *arrows* in (*C*) indicate the rearrangements of these residues. *D–E*, scatter plots of the distances between residues P7′-F995 and P6′-F1092, and the χ1 and χ2 dihedral angles of W1158, respectively, showing the upward movement of the TA in the binding pocket. *F*, SRE-luciferase assay for ADGRL3-CTF-nluc and mutant construct ADGRL3-W1158A-CTF-nluc. Statistics were calculated using an unpaired *t* test (***$p < 0.001$). *G*, Gβγ release testing ADGRL3-CTF and ADGRL3-W1158A-CTF activation of $G\alpha_{13}$. Statistics were calculated using an unpaired *t* test (***$p < 0.001$; ****$p < 0.0001$). *H*, the structure of the ADGRL1 GAIN domain (PDB 4DLQ) (5), with the TA highlighted with *dark gray*. *I*, a zoom-in view of the autoproteolysis site indicated by the dotted box in panel *H*. $F^{P3'}$ located at the turn between the last β-strand of the GPS and the TA is expected to stabilize the conformation necessary for the autoproteolysis occurring between L^{P1} and $T^{P1'}$; $T^{P1'}$ also forms a hydrophobic-aromatic interaction with the $F^{P3'}$, indicated by the *cyan* space-filling representation. The "*" indicates the location of autoproteolysis. *Orange* and *green* residues are those within 5 Å of $F^{P3'}$ and $L^{P6'}$, respectively. ADGRL3, adhesion G protein-coupled receptor latrophilin 3; CTF, C-terminal fragment; GAIN, GPCR autoproteolysis-inducing domain; GPS, GPCR proteolysis site; SRE, serum response element.

Biolabs). All engineered cDNAs were sequenced by Genewiz from Azenta Life Sciences.

Cell culture

HEK293T cells (American Type Culture Collection) and HEK293 cells with targeted deletion *via* CRISPR-Cas9 of *GNAS*, *GNAL*, *GNAQ*, *GNA11*, *GNA12*, *GNA13*, and *GNAZ* (HEKΔ7) (12) were maintained in high-glucose Dulbecco's modified Eagle's medium (DMEM) supplemented with 10% fetal bovine serum and 1% penicillin-streptomycin (10,000 U/ml) at 37 °C in a 5% CO_2 humidified incubator.

Gene expression assay

The experimental setup for this assay was described previously (7). Briefly, HEK293T cells were transfected with Lipofectamine 2000 (2.5 μl/1 μg cDNA) and Opti-MEM using two concentrations of ADGRL3 constructs (200 or 600 ng), 600 ng of reporter dual-glo SRE-luciferase/renilla plasmid (32), and balancer pcDNA5/FRT to 1200 ng. After 24 h, cells were aliquoted into a 96-well black/white isoplate (PerkinElmer Life Sciences) in technical replicates at 80 μl/well. Lysis buffer (40 μl/well) containing D-luciferin (NanoLight Technologies) was prepared as previously described (33). After 10 min, firefly

luciferase emission was read at 535 nm on a PHERAstar FS microplate reader (BMG LABTECH). *Renilla* salts buffer (60 μl/well) containing coelenterazine-*h* (NanoLight Technologies) was prepared as previously described (33). *Renilla* luciferase emission was read at 475 nm after 10 min. Data were normalized by dividing the 525 nm firefly emission by the 475 nm *Renilla* emission. Fold change was calculated by dividing these normalized values by the empty vector control.

For assays using the ADGRL3-CTF-nluc constructs, the cell media was exchanged to DMEM approximately 6 h after transfection. After 24 h, the media was aspirated from the cells, and each well was gently rinsed with Dulbecco's phosphate-buffered saline (DPBS). Cells were then mechanically detached using 200 μl DPBS, and 60 μl of the resuspension was distributed in triplicate to a 96-well black/white isoplate. Next, 30 μl of D-luciferin dissolved in the assay buffer was added to each well for a final concentration of 2 mM. Emission was read at 525 nm after 30 min incubation using a PHERAstar FS microplate reader.

BRET assay

The experimental setup for this assay was described previously (7). Briefly, HEKΔ7 cells were cotransfected with receptor cDNA (200 ng), Gα (0 or 720 ng), Gβ1 (250 ng), Gγ2-Venus (250 ng), membrane-anchored GRK3ct-Rluc8 (50 ng), and empty vector pCDNA5/FRT to 1470 ng. The transfected cells were resuspended after 24 h, and 45 μl/well was distributed into a 96-well OptiPlate black-white plate. Cells were incubated for 10 min with 10 μl coelenterazine-*h* (final 5 μM). Then, 45 μl/well of enterokinase (5.5 units) was added to initiate receptor cleavage. Donor (Rluc8) and acceptor (mVenus) emission were read using a PHERAstar FS microplate reader at 485 nm and 525 nm, respectively. The BRET signal was calculated as the ratio of light emitted at 525 nm over that emitted at 485 nm. Enterokinase-induced BRET was obtained by subtracting baseline BRET (DPBS) for each condition.

Surface expression measurements using SNAPfast-tag

HEK293T cells were seeded at a density of 900,000 cells/well in a 6-well plate. After 24 h, the cells were transfected using FuGENE transfection reagent (8 μl/2 μg cDNA) and Opti-MEM with SNAPfast-tagged receptor cDNA (2 μg). At 24 h posttransfection, cells were incubated with 500 μl 1 μM impermeant Janelia Fluor 646 dissolved in complete DMEM for 30 min. The cells were washed 3 times with complete DMEM and once with DPBS. Cells were then resuspended in 500 μl DPBS. The resuspension was added in technical replicates to a 96-well OptiPlate black plate (PerkinElmer Life Sciences) at a volume of 100 μl/well. Emission was read using a PHERAstar FS microplate reader with the filter 640/680 at a gain of 2000.

Immunoblot analysis

HEK293T cells were seeded in a 6-well plate at a density of 400,000 cells/ml. After 24 h, cells were transfected with receptor cDNA (2 μg) using FuGENE transfection reagent (8 μl/2 μg cDNA) and Opti-MEM. After 24 h, cells were placed on ice and lysed with 500 μl RIPA buffer for 30 min. After lysis, cells were detached and spun at 15,000*g* for 30 min at 4 °C to pellet debris. Cells were then treated at 37 °C for 1 h with PNGase F (New England Biolabs). Then, 60 μl of PNGase-treated lysate was transferred to a 1.5 ml microcentrifuge tube containing 60 μl 2X SDS Laemmli sample buffer (Sigma-Aldrich). Proteins were then separated *via* SDS-PAGE (Mini-PROTEAN TGX, 4–15%, Bio-Rad Laboratories, Inc). The gel was then transferred to a PVDF membrane (Immobilon-P Membrane, Merck Millipore Ltd) and placed in a 5% milk tris-buffered saline with 0.1% tween-20 (TBS-T) solution for 1 h at RT. The membrane was washed 5 × 5 min in TBS-T and incubated at 4 °C overnight with 1° rabbit anti-FLAG antibody (1:500, Thermo Fisher Scientific, PA1-984B). Following this incubation, the membrane was washed 5 × 5 min in TBS-T and then incubated for 1 h with 2° anti-rabbit HP antibody (1:10,000, Thermo Fisher Scientific, Cat #31458). The membrane was then washed 5 × 5 min with TBS-T and incubated with SuperSignal West Pico Chemiluminescent Substrate (Thermo Fisher Scientific). Bands were visualized using an Azure Biosystems c600 Imaging System (Azure Biosystems Inc).

Molecular modeling and MD simulations

The cryo-EM structure of human ADGRL3 in complex with $G_{\alpha 13}$ protein (PDB 7SF7) (8) was used as the structural template to build the homology model of the mouse ADGRL3/$G_{\alpha 13}$ complex with MODELLER (version 10.0) (34). The resulting model with the lowest DOPE score was selected. Based on the pKa prediction with PROPKA for the titratable residues, which found the side chain (35) carboxyl group of Glu992 of ADGRL3 to have a pKa of 8.02, we protonated Glu992 to its neutral form. The N-terminus of the tethered peptide of ADGRL3 was neutrally capped with NH_2-. To assemble the MD simulation systems for both of the ADGRL3/$G_{\alpha 13}$ complexes (WT and $L^{P6'}A/M^{P7'}A$ mutant), the CHARMM-GUI server (36) was used to embed each complex in a 1-palmitoyl-2-oleoyl-sn-glycero-3-phosphocholine (POPC) bilayer with a water phase on both sides. Na^+ and Cl^- were added to neutralize the system and to reach a final concentration of 0.15 M. Each simulation system includes ∼137,000 atoms and has equilibrated dimensions of ∼101 × 101 × 131 $Å^3$.

The MD simulations were carried out using NAMD 2.14 (37) with the CHARMM36 m force field for both protein and POPC (31, 32), and the TIP3 model (38) for water. The NPγT ensemble was used at constant temperature (310 K) maintained with Langevin dynamics and 1 atm constant pressure achieved with the hybrid Nose–Hoover Langevin piston method (39) on an anisotropic flexible periodic cell with a constant-ratio constraint applied in the X – Y plane. Simulations were performed with a cutoff of 12 Å for the nonbonded interactions. The particle mesh Ewald method (40) was used to evaluate long-range electrostatic effects. The systems were initially minimized for 10,000 steps and then equilibrated with

restraints on the protein heavy atoms for 1875 ps. The time step of 1 fs was used for the first 375 ps, which was then increased to 2 fs for the rest of simulations. Another 30 ns equilibrating simulation with restraints only on the protein backbone atoms was performed afterward. All restraints on the receptor were released in production runs. We collected six WT and five mutant MD simulation trajectories starting from different random number seeds, resulting in total simulation lengths of 1893 and 1998 ns, respectively.

In-house python scripts and MD analysis (41) were used to process the trajectories and calculate the geometric measures shown in Figure 5. The distances of L/A$^{P6'}$-F1092 and M/A$^{P7'}$-F995 are the minimum distances between the backbone heavy atoms of residues P6′ or P7′ and the sidechain heavy atoms of F995 or F1092.

Data availability

Data will be shared upon request. Contact the corresponding author here: jaj2@cumc.columbia.edu.

Acknowledgments—We thank Dr Demet Araç-Ozkan (University of Chicago, IL) for the generous gift of the Dual-Glo SRE-luciferase reporter plasmid, Dr Luke Lavis (Janelia Research Campus) for supplying the Fluor 646 dye, and Dr Asuka Inoue (Tohoku University, Japan) for the HEKΔ7 cell line. This work utilized the computational resources of the NIH HPC Biowulf cluster (http://hpc.nih.gov).

Author contributions—N. A. P.-H. and J. A. J. conceptualization; N. A. P.-H. formal analysis; L. S. software; L. S. and J. A. J. supervision; L. S. and J. A. J. funding acquisition; N. A. P.-H. validation; N. A. P.-H. visualization; N. A. P.-H., M. W. V. D., and K. H. L. investigation; N. A. P.-H. and L. S. methodology; N. A. P.-H., M. W. V. D., K. H. L., L. S., and J. A. J. writing–original draft; N. A. P.-H., M. W. V. D., K. H. L., and J. S. and J. A. J. writing–review & editing.

Funding and additional information—This work was supported by T32 MH015144 (N. A. P.-H.) and MH054137, the Hope for Depression Research Foundation and Miriam's Magical Memorial Mission (J. A. J.). This work was partially supported by the National Institute on Drug Abuse—Intramural Research Program (Z1A DA000606, L. S.). The content is solely the responsibility of the authors and does not necessarily represent the official views of the National Institutes of Health.

Conflict of interest—The authors declare that they have no conflicts of interest with the contents of this article.

Abbreviations—The abbreviations used are: ADGRLs, adhesion G protein-coupled receptor latrophilins; aGPCR, adhesion G protein-coupled receptor; BRET, bioluminescence resonance energy transfer; CTF, C-terminal fragment; DPBS, Dulbecco's phosphate-buffered saline; FL, full-length; GPCR, G protein-coupled receptor; GAIN, GPCR autoproteolysis-inducing domain; GPS, GPCR proteolysis site; NTF, N-terminal fragment; SRE, serum response element; TA, tethered agonist; TBS-T, tris-buffered saline with 0.1% tween-20; 7TM, seven transmembrane.

References

1. Silva, J.-P., Lelianova, V. G., Ermolyuk, Y. S., Vysokov, N., Hitchen, P. G., Berninghausen, O., *et al.* (2011) Latrophilin 1 and its endogenous ligand Lasso/teneurin-2 form a high-affinity transsynaptic receptor pair with signaling capabilities. *Proc. Natl. Acad. Sci. U. S. A.* **108**, 12113–12118
2. O'Sullivan, M. L., de Wit, J., Savas, J. N., Comoletti, D., Otto-Hitt, S., Yates, J. R., *et al.* (2012) FLRT proteins are endogenous latrophilin ligands and regulate excitatory synapse development. *Neuron* **73**, 903–910
3. Moreno-Salinas, A. L., Avila-Zozaya, M., Ugalde-Silva, P., Hernández-Guzmán, D. A., Missirlis, F., and Boucard, A. A. (2019) Latrophilins: a neuro-centric view of an evolutionary conserved adhesion G protein-coupled receptor subfamily. *Front Neurosci.* **13**, 700
4. Vizurraga, A., Adhikari, R., Yeung, J., Yu, M., and Tall, G. G. (2020) Mechanisms of adhesion G protein-coupled receptor activation. *J. Biol. Chem.* **295**, 14065–14083
5. Araç, D., Boucard, A. A., Bolliger, M. F., Nguyen, J., Soltis, S. M., Südhof, T. C., *et al.* (2012) A novel evolutionarily conserved domain of cell-adhesion GPCRs mediates autoproteolysis. *EMBO J.* **31**, 1364–1378
6. Liebscher, I., and Schöneberg, T. (2016) Tethered agonism: a common activation mechanism of adhesion gpcrs. *Handb. Exp. Pharmacol.* **234**, 111–125
7. Mathiasen, S., Palmisano, T., Perry, N. A., Stoveken, H. M., Vizurraga, A., McEwen, D. P., *et al.* (2020) G12/13 is activated by acute tethered agonist exposure in the adhesion GPCR ADGRL3. *Nat. Chem. Biol.* **16**, 1343–1350
8. Barros-Álvarez, X., Nwokonko, R. M., Vizurraga, A., Matzov, D., He, F., Papasergi-Scott, M. M., *et al.* (2022) The tethered peptide activation mechanism of adhesion GPCRs. *Nature* **604**, 757–762
9. [preprint] Kordon, S. P., Dutka, P., Adamska, J. M., Bandekar, S. J., Leon, K., Adams, B., *et al.* (2022) Isoform- and ligand-specific modulation of the adhesion GPCR ADGRL3/Latrophilin3 by a synthetic binder. *biorxiv.* https://doi.org/10.1101/2022.07.20.500857
10. Hollins, B., Kuravi, S., Digby, G. J., and Lambert, N. A. (2009) The c-terminus of GRK3 indicates rapid dissociation of G protein heterotrimers. *Cell Signal* **21**, 1015–1021
11. Lizano, E., Hayes, J. L., and Willard, F. S. (2021) A synthetic method to assay adhesion-family G-protein coupled receptors. Determination of the G-protein coupling profile of ADGRG6(GPR126). *Biochem. Biophys. Res. Commun.* **534**, 317–322
12. Alvarez-Curto, E., Inoue, A., Jenkins, L., Raihan, S. Z., Prihandoko, R., Tobin, A. B., *et al.* (2016) Targeted elimination of G proteins and arrestins defines their specific contributions to both intensity and duration of G protein-coupled receptor signaling. *J. Biol. Chem.* **291**, 27147–27159
13. Keppler, A., Kindermann, M., Gendreizig, S., Pick, H., Vogel, H., and Johnsson, K. (2004) Labeling of fusion proteins of O6-alkylguanine-DNA alkyltransferase with small molecules *in vivo* and *in vitro*. *Methods* **32**, 437–444
14. Keppler, A., Pick, H., Arrivoli, C., Vogel, H., and Johnsson, K. (2004) Labeling of fusion proteins with synthetic fluorophores in live cells. *Proc. Natl. Acad. Sci. U. S. A.* **101**, 9955–9959
15. Shi, L., Liapakis, G., Xu, R., Guarnieri, F., Ballesteros, J. A., and Javitch, J. A. (2002) Beta2 adrenergic receptor activation. Modulation of the proline kink in transmembrane 6 by a rotamer toggle switch. *J. Biol. Chem.* **277**, 40989–40996
16. Regan, S. L., Hufgard, J. R., Pitzer, E. M., Sugimoto, C., Hu, Y.-C., Williams, M. T., *et al.* (2019) Knockout of latrophilin-3 in Sprague-Dawley rats causes hyperactivity, hyper-reactivity, under-response to amphetamine, and disrupted dopamine markers. *Neurobiol. Dis.* **130**, 104494
17. Mortimer, N., Ganster, T., O'Leary, A., Popp, S., Freudenberg, F., Reif, A., *et al.* (2019) Dissociation of impulsivity and aggression in mice deficient for the ADHD risk gene Adgrl3: evidence for dopamine transporter dysregulation. *Neuropharmacology* **156**, 107557
18. Wallis, D., Hill, D. S., Mendez, I. A., Abbott, L. C., Finnell, R. H., Wellman, P. J., *et al.* (2012) Initial characterization of mice null for Lphn3, a gene implicated in ADHD and addiction. *Brain Res.* **1463**, 85–92

19. van der Voet, M., Harich, B., Franke, B., and Schenck, A. (2016) ADHD-associated dopamine transporter, latrophilin and neurofibromin share a dopamine-related locomotor signature in Drosophila. *Mol. Psychiatry* **21**, 565–573
20. Orsini, C. A., Setlow, B., DeJesus, M., Galaviz, S., Loesch, K., Ioerger, T., *et al.* (2016) Behavioral and transcriptomic profiling of mice null for Lphn3, a gene implicated in ADHD and addiction. *Mol. Genet. Genomic Med.* **4**, 322–343
21. Regan, S. L., Cryan, M. T., Williams, M. T., Vorhees, C. V., and Ross, A. E. (2020) Enhanced transient striatal dopamine release and reuptake in lphn3 knockout rats. *ACS Chem. Neurosci.* **11**, 1171–1177
22. Lange, M., Norton, W., Coolen, M., Chaminade, M., Merker, S., Proft, F., *et al.* (2012) The ADHD-linked gene Lphn3.1 controls locomotor activity and impulsivity in zebrafish. *Mol. Psychiatry* **17**, 855
23. Jackson, V. A., del Toro, D., Carrasquero, M., Roversi, P., Harlos, K., Klein, R., *et al.* (2015) Structural basis of latrophilin-FLRT interaction. *Structure* **23**, 774–781
24. Del Toro, D., Carrasquero-Ordaz, M. A., Chu, A., Ruff, T., Shahin, M., Jackson, V. A., *et al.* (2020) Structural basis of teneurin-latrophilin interaction in repulsive guidance of migrating neurons. *Cell* **180**, 323–339.e19
25. Lu, Y. C., Nazarko, O. V., Sando, R., Salzman, G. S., Li, N.-S., Südhof, T. C., *et al.* (2015) Structural basis of latrophilin-FLRT-UNC5 interaction in cell adhesion. *Structure* **23**, 1678–1691
26. Pederick, D. T., Lui, J. H., Gingrich, E. C., Xu, C., Wagner, M. J., Liu, Y., *et al.* (2021) Reciprocal repulsions instruct the precise assembly of parallel hippocampal networks. *Science* **372**, 1068–1073
27. Bridges, J. P., Safina, C., Pirard, B., Brown, K., Filuta, A., Panchanathan, R., *et al.* (2022) Regulation of pulmonary surfactant by the adhesion GPCR GPR116/ADGRF5 requires a tethered agonist-mediated activation mechanism. *Elife* **11**, e69061
28. Sakurai, T., Kamakura, S., Hayase, J., Kohda, A., Nakamura, M., and Sumimoto, H. (2022) GPR125 (ADGRA3) is an autocleavable adhesion GPCR that traffics with Dlg1 to the basolateral membrane and regulates epithelial apico-basal polarity. *J. Biol. Chem.* **298**, 102475
29. [preprint] Pederick, D. T., Perry-Hauser, N. A., Meng, H., He, Z., Javitch, J. A., and Luo, L. (2022) Context-dependent requirement of G protein coupling for Latrophilin-2 in target selection of hippocampal axons. *biorxiv*. https://doi.org/10.1101/2022.09.26.509559
30. Kishore, A., Purcell, R. H., Nassiri-Toosi, Z., and Hall, R. A. (2016) Stalk-dependent and stalk-independent signaling by the adhesion G protein-coupled receptors GPR56 (ADGRG1) and Bai1 (ADGRB1). *J. Biol. Chem.* **291**, 3385–3394
31. Beliu, G., Altrichter, S., Guixà-González, R., Hemberger, M., Brauer, I., Dahse, A.-K., *et al.* (2021) Tethered agonist exposure in intact adhesion/class B2 GPCRs through intrinsic structural flexibility of the GAIN domain. *Mol. Cell* **81**, 905–921.e5
32. Nazarko, O., Kibrom, A., Winkler, J., Leon, K., Stoveken, H., Salzman, G., *et al.* (2018) A comprehensive mutagenesis screen of the adhesion GPCR latrophilin-1/ADGRL1. *iScience* **3**, 264–278
33. Baker, J. M., and Boyce, F. M. (2014) High-throughput functional screening using a homemade dual-glow luciferase assay. *J. Vis. Exp.*, 50282
34. Webb, B., and Sali, A. (2021) Protein structure modeling with MODELLER. *Methods Mol. Biol.* **2199**, 239–255
35. Olsson, M. H. M., Søndergaard, C. R., Rostkowski, M., and Jensen, J. H. (2011) PROPKA3: consistent treatment of internal and surface residues in empirical pK predictions. *J. Chem. Theor. Comput.* **7**, 525–537
36. Wu, E. L., Cheng, X., Jo, S., Rui, H., Song, K. C., Dávila-Contreras, E. M., *et al.* (2014) CHARMM-GUI Membrane Builder toward realistic biological membrane simulations. *J. Comput. Chem.* **35**, 1997–2004
37. Phillips, W. J., Wong, S. C., and Cerione, R. A. (1992) Rhodopsin/transducin interactions. II. Influence of the transducin-beta gamma subunit complex on the coupling of the transducin-alpha subunit to rhodopsin. *J. Biol. Chem.* **267**, 17040–17046
38. Jorgensen, W. L., Chandrasekhar, J., Madura, J. D., Impey, R. W., and Klein, M. L. (1983) Comparison of simple potential functions for simulating liquid water. *J. Chem. Phys.* **79**, 926
39. Grønbech-Jensen, N., and Farago, O. (2014) Constant pressure and temperature discrete-time Langevin molecular dynamics. *J. Chem. Phys.* **141**, 194108
40. Darden, T., York, D., and Pedersen, L. (1993) Particle mesh Ewald: an N·log(N) method for Ewald sums in large systems. *J. Chem. Phys.* **98**, 10089
41. Michaud-Agrawal, N., Denning, E. J., Woolf, T. B., and Beckstein, O. (2011) MDAnalysis: a toolkit for the analysis of molecular dynamics simulations. *J. Comput. Chem.* **32**, 2319–2327